

# The annular gap model for gamma-ray emission from young and millisecond pulsars

Y. J. Du<sup>1\*</sup>, G. J. Qiao<sup>2</sup>, J. L. Han<sup>1</sup>, K. J. Lee<sup>2,3,4</sup> and R. X. Xu<sup>2</sup>

<sup>1</sup>National Astronomical Observatories, Chinese Academy of Sciences, Jia-20, Datun Road, Chaoyang District, Beijing 100012, China

<sup>2</sup>Department of Astronomy, Peking University, Beijing 100871, China

<sup>3</sup>The University of Manchester, School of Physics and Astronomy, Jodrell Bank Centre for Astrophysics, Alan Turing Building, Manchester, M13 9PL, UK

<sup>4</sup>Max-Planck-Institut für Radioastronomie, Auf dem Hügel 69, 53121 Bonn, Germany

1 November 2021

## ABSTRACT

Pulsed high energy radiation from pulsars is not yet completely understood. In this paper, we use the 3D self-consistent annular gap model to study light curves for both young and millisecond pulsars observed by the Fermi Gamma-ray Space Telescope. The annular gap can generate high energy emission for short-period pulsars. The annular gap regions are so large that they have enough electric potential drop to accelerate charged particles to produce gamma-ray photons. For young pulsars, the emission region is from the neutron star surface to about half of the light cylinder radius, and the peak emissivity is in the vicinity of the null charge surface. The emission region for the millisecond pulsars is located much lower than that of the young pulsars. The higher energy  $\gamma$ -ray emission comes from higher altitudes in the magnetosphere. We present the simulated light curves for three young pulsars (the Crab, the Vela, the Geminga) and three millisecond pulsars (PSR J0030+0451, PSR J0218+4232, PSR J0437-3715) using the annular gap model. Our simulations can reproduce the main properties of observed light curves.

**Key words:** Radiation mechanisms: non-thermal – Pulsars: individual: Crab, Vela, Geminga, J0030+0451, J0218+4232, J0437-4715 – Gamma-rays: stars.

## 1 INTRODUCTION

Pulsars are fascinating astronomical objects in the universe. After more than 40 years since the discovery of the first pulsars, their pulsed non-thermal emission has not been completely understood due to the insufficient knowledge about the global acceleration electric field and particle dynamics in the magnetosphere.

High energy emission (e.g.  $\gamma$ -ray emission) from pulsars takes away a significant fraction of the rotational energy. Several space telescopes were used to observe high energy emission from pulsars. Six  $\gamma$ -ray pulsars and three candidates were discovered by the Energetic Gamma Ray Experiment Telescope (EGRET) (Thompson et al. 1999). One young pulsar (PSR B1509-58) was detected only up to 10 MeV by the Imaging Compton Telescope (COMPTEL) (Thompson 2001). Pulsars detected by EGRET show double peaks with bridge emission. Thanks to the launching of Astro-rivelatore Gamma a Immagini LEggero (AGILE) and Fermi Gamma-ray Space Telescope (FGST), more than forty new  $\gamma$ -ray pulsars have been discovered in the last year, including gamma-ray only pulsars and a new population of millisecond pulsars (Pellizzoni et al. 2009, Abdo et al. 2009b, Abdo et al. 2009c). With these data, we have good opportunities to study the open questions, e.g., the location of the emission zones, possible particle dynamics in the magnetosphere and so on. Theory on non-thermal high energy emission from pulsars should be significantly improved in the coming years.

Physical and geometric magnetosphere models have been proposed to explain pulsar's  $\gamma$ -ray radiation, as we will summarize below, differing on the acceleration region of the primary particles and the mechanism for the production of the high energy photons.

The first is the polar cap model (Daugherty & Harding 1982, Daugherty & Harding 1994, Daugherty & Harding 1996). The acceleration region is located in the vicinity of neutron star surface up to tens of kilometers near the magnetic pole. The observed phase-resolved spectra

\* E-mail: dyj@nao.cas.cn.

of  $\gamma$ -ray pulsars can also be modeled. This model favors a small inclination angle, e.g., a nearly aligned rotator. The  $\gamma$ -ray emission region is so close to the neutron star surface that high energy  $\gamma$ -ray photons could be absorbed in the strong magnetic field (Lee et al. 2010).

The polar cap model was combined with the slot gap model recently to explain the pulsar  $\gamma$ -ray radiation (Muslimov & Harding 2003, Muslimov & Harding 2004). A 3D model of optical-to- $\gamma$ -ray emission from the slot gap was developed to study the Crab pulsar's light curve, phase-averaged and phase-resolved spectrum (Harding et al. 2008). Hirotani (2008) demonstrated that the slot gap model reproduces at most 20% of the observed fluxes because of the small trans-field thickness. The two-pole caustic model is proposed by Dyks & Rudak (2003). The gap is thin, confined to the surface of the last open field lines, and extends from both polar caps to the light cylinder. Double peak light curve with a large peak separation (e.g., Vela) can be well reproduced by this model. But this model has difficulties in explaining the light curves with small peak separations (e.g., B1706-44 and B1055-52). Frackowiak & Rudak (2005) presented spectral and light curve properties of gamma radiation obtained by numerical modeling of some pulsars, i.e. PSR J0218+4232, PSR J0437-4715 and PSR B1821-24.

The outer gap model is another excellent model to interpret  $\gamma$ -ray emission from pulsars (Cheng, Ho & Ruderman 1986a, Cheng, Ho & Ruderman 1986b, Chiang & Romani 1992, Romani & Yadigaroglu 1995, Romani 1996, Zhang & Cheng 1997, Cheng, Ruderman & Zhang 2000, Zhang et al. 2004, Lin & Zhang 2009). The classical outer gap starts at the null charge surface (inner boundary), ends at the light cylinder (outer boundary); it is further bounded by the last open field line (lower boundary) and a layer of electric current (upper boundary). However, Hirotani et al. (2003) argued that the position of the inner boundary could be shifted towards the neutron star surface because a current at nearly the Goldreich-Julian rate (Goldreich & Julian 1969) is injected to the outer gap. Tang et al. (2008) used this modified outer gap to study the multifrequency phase-resolved spectra of the Crab pulsar.

Watters et al. (2009) have simulated a population of young pulsars and computed the beaming pattern and light curves for the three models: the polar cap model, the two-pole caustic (slot gap) model and the outer gap model. Venter et al. (2009) presented light curves of millisecond pulsars from 3D emission modeling, in the geometric context of the polar cap, the outer gap, and the two-pole caustic models. They found that most of the light curves are best fit by the two-pole caustic and the outer gap models, which indicates the presence of narrow accelerating gaps limited by robust pair production – even in these pulsars with very low spin-down luminosities.

Force-free relativistic MHD were used to study the time-dependent evolution and dynamics of pulsar magnetospheres for either aligned or oblique magnetic geometries (Contopoulos et al. 1999, Komissarov 2006, Spitkovsky 2006, McKinney 2006, Timokhin 2006 and Gruzinov 2007). Recent efforts on theoretical understanding the high energy emission from pulsars can be found from Bai & Spitkovsky (2009a; 2009b). They modeled gamma-ray pulsar light curves for the two-pole caustic model (slot gap model), the outer gap model and the “separatrix layer” model using the more realistic magnetic field taken from 3D force-free magnetospheric simulations. Their separatrix layer model might be associated with the current sheet beyond the light cylinder. Their simulated results indicate that the separatrix layer model can best reproduce the observations.

The annular gap model we are developing is originally proposed by Qiao et al. (2004) and Qiao et al. (2007). The gap region is located between the critical field lines<sup>1</sup> and last open field lines, and extends from the neutron star surface to the light cylinder. The region for high energy emission in the annular gap model is concentrated in the vicinity of the null charge surface, i.e., an intermediate emission height, different from the outer gap model. The annular gap has a sufficient thickness of trans-field lines and a wide altitude range for particle acceleration. The role of the annular gap depends on the mono-polar voltage in the annular region, so it is favorable for short period pulsars. This model combines the advantages of the polar gap, the slot gap and the outer gap models, and works well for pulsars with short spin periods. It is a promising model to explain high energy emission from young and millisecond pulsars.

In this paper, we focus on the  $\gamma$ -ray light curves for young and millisecond pulsars in the framework of the annular gap model. In § 2, detailed physics and geometry of the annular gap are introduced. The results of simulated photon sky-maps and light curves for young and millisecond pulsars are presented in § 3. Discussions and conclusions are given in § 4.

## 2 THE ANNULAR GAP MODEL: PHYSICS AND GEOMETRY

The open field line region of a pulsar magnetosphere can be divided into two parts by the critical field lines. One is the annular region, which is between critical field lines and last open field lines. The other is the core region, which is within the critical field lines. Taking an anti-parallel rotator as an example, the radii of the core polar region ( $r_{\text{core}}$ ) and the full polar cap region ( $r_{\text{p}}$ ) are  $r_{\text{core}} = (2/3)^{3/4} R(\Omega R/c)^{1/2}$  and  $r_{\text{p}} = R(\Omega R/c)^{1/2}$ , respectively (Ruderman & Sutherland 1975), here  $R$  is the pulsar's radius,  $\Omega$  is the angular spin frequency. The radius of the annular polar region is  $r_{\text{ann}} = r_{\text{p}} - r_{\text{core}} = 0.26R(\Omega R/c)^{1/2}$ . If pulsar's spin period is smaller, the annular radius ( $r_{\text{ann}}$ ) is larger. Therefore, the annular acceleration region is more important for those pulsars with a short spin period (e.g., millisecond and young pulsars) and is negligible for older pulsars with a large spin period.

If pulsars are bare quark stars (Xu 2002, 2005), then two kinds of acceleration regions could be formed, namely, the inner vacuum core gap and inner vacuum annular gap. If pulsars are neutron stars with enough surface binding energy, the inner vacuum core gap (Ruderman & Sutherland 1975) can be formed for an inclined rotator with a magnetic inclination angle  $\alpha > 90^\circ$ ; while the inner vacuum annular gap (Qiao et al. 2004) can be formed only for an inclined rotator with a magnetic inclination angle  $\alpha < 90^\circ$ . If the binding energy of a neutron star's surface is not high enough, both negative and positive charges will flow out freely from the surface. Then two kinds of acceleration

<sup>1</sup> The critical field line is across the intersection of the null charge surface and light cylinder.

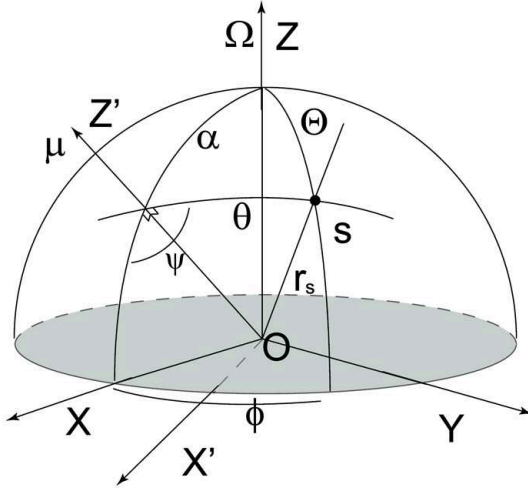


**Figure 1.** The coordinate systems for an oblique rotator. In the laboratory frame  $O - XYZ$ , the  $Z$  axis is aligned with the rotational axis  $\Omega$

of a pulsar. The magnetic frame  $O - X'YZ'$  is generated by rotating the  $O - XYZ$  coordinates around  $Y$  axis by an inclination angle of  $\alpha$ , the  $Z'$  axis is aligned with the dipolar magnetic moment  $\mu$ . Point “s” is an emitting source on an arbitrary magnetic field line. The  $r_s$  is the altitude of the radiation source from the neutron star center. The polar angle and azimuthal angle in laboratory polar coordinates are denoted as  $\Theta, \phi$ , while the polar angle and azimuthal angle in the magnetic polar coordinates are  $\theta, \psi$ .

regions (annular and core) could be formed. Particle acceleration is more effective in the annular gap region. The annular acceleration region extends from the pulsar surface to the null charge surface or even beyond it. This leads to a fan-beam  $\gamma$ -ray emission, which is suitable to interpret the observed light curves and the broad-band emission (Qiao et al. 2007).

## 2.1 Coordinates for the Annular Gap

As shown in Fig.1, in the coordinate  $O - XYZ$  of the laboratory frame, the  $Z$  axis is aligned with the rotational axis  $\Omega$  of the pulsar. The magnetic frame  $O - X'YZ'$  is generated by rotating the  $O - XYZ$  coordinate around  $Y$  axis by the inclination angle  $\alpha$ , the  $Z'$  axis is aligned with the dipolar magnetic moment  $\mu$ . The two vectors  $\Omega$  and  $\mu$  locates in the plane  $O - XZ$ , which is called the  $\Omega - \mu$  plane. The polar coordinate associated with  $O - XYZ$  and  $O - X'YZ'$  are called the laboratory polar coordinate and the magnetic polar coordinate, respectively. The polar angle and azimuthal angle in the laboratory polar coordinate are denoted as  $\Theta, \phi$ , while the polar angle and azimuthal angle in the magnetic polar coordinate as  $\theta, \psi$ . Similar to Lee et al. (2010), we use bold type to label the vector or the matrix; while we use subscripts  $x, y, z$  and  $x', y', z'$  to indicate their components in the laboratory frame and the magnetic coordinate, respectively.

## 2.2 Geometry, emission region and modeling

We assume that pulsars have a dipole magnetic field in the magnetic nonrotating frame. Thus dipole field line function can be expressed as

$$r = R_e \sin^2 \theta, \quad (1)$$

where  $r$  is the polar radius from pulsar center to an emission point;  $R_e$  is the maximum radius of the field line, which is the function of  $\alpha$  and  $\psi_s$ . To obtain the field line constant  $R_e$  for the last open field line, Zhang et al. (2007) and Lee et al. (2009) derived a cubic equation, i.e.,

$$A \cot^3 \theta_M + B \cot^2 \theta_M + C \cot \theta_M + D = 0, \quad (2)$$

where  $A = 4 \sin^2 \alpha$ ,  $B = 5 \sin 2\alpha \cos \psi_s$ ,  $C = 4 \sin^2 \alpha - 6(\sin^2 \alpha \cos^2 \psi_s - \cos^2 \alpha)$ ,  $D = -\sin 2\alpha \cos \psi_s$ ,  $\theta_M$  is the polar angle at point M. Therefore  $\cot \theta_M$  can be determined analytically, and  $R_e$  is

$$R_e(\alpha, \psi_s) = \frac{R_{LC}(1 + \cot^2 \theta_M)^{3/2}}{\sqrt{1 + \cot^2 \theta_M - (\cos \alpha \cot \theta_M - \sin \alpha \cos \psi_s)^2}}, \quad (3)$$

where  $R_{LC}$  is the radius of light cylinder. Given the values of  $R_e$  and  $\psi_s$ , the last open magnetic field line can be uniquely defined. The polar angle  $\theta_N$  of the null charge surface (defined as  $\Omega \cdot \mathbf{B} = 0$ ) is given by

$$\theta_N = \frac{1}{2} \arccos\left(\frac{\sqrt{8 \cot^2 \alpha \sec^2 \psi_s + 9} \pm \cot^2 \alpha \sec^2 \psi_s}{3 \cot^2 \alpha \sec^2 \psi_s + 3}\right). \quad (4)$$

For a critical field line, which is across the intersection of the null charge surface and light cylinder, there is a relation between  $\Theta_N$  and  $\theta_N$  (Gangadhara 2004, Wang et al. 2006), i.e.

$$\Theta_N = \arccos(\cos \alpha \cos \theta_N - \sin \alpha \sin \theta_N \cos \psi_s). \quad (5)$$

Then, the critical field line constant,  $R_{e,N}$ , is given by

$$R_{e,N}(\alpha, \psi_s) = R_{LC} \csc^2 \theta_N \csc \theta_N. \quad (6)$$

The height of the null charge surface on the last open field line can be derived, i.e.  $r_N(\psi_s) = R_e(\alpha, \psi_s) \sin^2 \theta_N$ . Qiao et al. (2007) gave an one-dimension solution to the acceleration electric field, the true 3D solution for the Poisson equation with mixed boundary conditions is unknown.

Dyks & Harding (2004) found that, at low altitudes, a distorted angle of the order of  $(r/R_{LC})^2$  is attributed to the rotation deflection on the local direction of the magnetic field, where  $r$  is the radial distance of the emission source. In the annular gap model, the radiation region is concentrated on the vicinity of the null charge surface of the last open field lines, the emission height is well below the light cylinder radius  $R_{LC}$ , and the sweepback effect on open field lines could be ignored. We use the 3D vacuum static dipolar field in this paper. Adopting the method of the open volume coordinates (Cheng et al. 2000, Dyks & Harding 2004, Tang et al. 2008, Harding et al. 2008), we calculate the polar shape of the annular gap. The inner edge and outer edge of the annular gap region are defined as the footpoints of the critical field lines and last open field lines. Here we adopt the conventional wisdom and assume that the  $\gamma$ -ray emissivities  $I(\theta_s, \psi_s)$  on each open field line has a Gaussian distribution, i.e.,

$$I(\theta_s, \psi_s) = I_{\text{peak}}(\theta_{\text{peak}}, \psi_s) \exp \left[ -\frac{(L(\theta_s, \psi_s) - L_0(\theta_{\text{peak}}, \psi_s))^2}{2\sigma^2} \right], \quad (7)$$

where  $L(\theta_s, \psi_s) = \int_0^{\theta_s} \sqrt{r^2 + (dr/d\theta)^2} d\theta$  is the arc length of the emission point on each field line counted from the pulsar center,  $\sigma$  is a bunch scale of the emission region on each open field line in the annular gap, and  $L_0(\theta_{\text{peak}}, \psi_s)$  is the arc length of the peak emissivity spot  $P(\theta_{\text{peak}}, \psi_s)$  on this open field line. In principle, the  $P(\theta_{\text{peak}}, \psi_s)$  could be located at anywhere on this field line. However, we found that our 1-D solution to the acceleration electric potential of each open field lines in the annular gap reaches the maximum near the null charge surface. The peak emissivity of the charged particles accelerated by the magnetospheric electric field then should be located near the null charge surface, which is also proved by our simulated light curves (See figures in §3).

The dominated emission region is located near the null charge surface (Qiao et al. 2004). The heights  $r_{\text{peak}}$  for the peak emissivity spot on each open field line (with the same  $\psi_s$ , different polar angle  $\theta$ ) in the annular gap can be written as

$$r_{\text{peak}}(\psi_s) = \lambda \kappa r_N(\psi_s) + (1 - \lambda) \kappa r_N(0), \quad (8)$$

where  $\kappa$  is a model parameter for the ratio of the peak emission height with respect to the null charge surface height  $r_N(\psi_s)$ ;  $\lambda$  is another model parameter, describing the deformation of emission location from a circle (Lee et al. 2006);  $r_N(0)$  is the height of the point with magnetic azimuthal  $\psi = 0^\circ$  on the last open field line. Then the peak emission position  $P$  on each open field line can be uniquely determined, i.e.,  $\theta_{\text{peak}} = \arcsin(\sqrt{r_{\text{peak}}/R_{e,f}(\alpha, \psi_s)})$ , where  $R_{e,f}(\alpha, \psi_s)$  is the field line constant of the open field line with  $\psi_s$ .

The peak emissivity  $I_{\text{peak}}(\theta_{\text{peak}}, \psi_s)$  for different open field lines could follow a Gaussian distribution (Cheng et al. 2000, Dyks & Rudak 2003), i.e.,

$$I_{\text{peak}}(\theta_{\text{peak}}, \psi_s) = I_0 \exp \left[ -\frac{(\theta_{\text{sp}}(\psi_s) - \theta_{\text{cp}}(\psi_s))^2}{\sigma_{\text{peak}}^2} \right], \quad (9)$$

where  $I_0$  is a scaled emissivity,  $\theta_{\text{sp}}$  is used to label a field line in the pulsar annular regions,  $\theta_{\text{cp}} = (\theta_N, \psi_s + \theta_{P, \psi_s})/2$  is the central field line among those field lines with  $\psi_s$ . During simulations, we take the width  $\sigma_{\text{peak}} \sim 0.002$  for young pulsars, and  $\sim 0.008$  for millisecond pulsars.

To calculate the light curves for a pulsar, we divide the polar shape of the annular gap into 31 rings and obtain the open field line with  $\psi_s$  and  $\theta_s$ . Then we calculate the emissivities projected onto the sky  $I(\theta_j, \psi_j)$  and direction  $\mathbf{n}_B(\theta_j, \psi_j)$  of the emission spot  $(\theta_j, \psi_j)$  on each open field line of each ring in the magnetic frame. We also take the aberration effect into account, and use the Lorentz transformation matrix to transform the emission direction  $\mathbf{n}_B(\theta_j, \psi_j)$  to the direction  $\mathbf{n}_\nu(\phi_j, \zeta_j)$  in the lab frame (observer frame), where  $\phi_j = \arctan(n_{\nu,y}/n_{\nu,x})$  is the emission spot's rotation phase with respect to the pulsar rotation axis, and  $\zeta_j = \arccos(n_{\nu,z}/\sqrt{n_{\nu,x}^2 + n_{\nu,y}^2 + n_{\nu,z}^2})$  the viewing angle for a distant, nonrotating observer (See details for aberration effect in Lee et al. 2010). We also add the phase shift  $\delta\phi_{\text{ret}} = r_n \cos(\theta_{\mu,j} - \theta_j)$ , the first order of equation (33) in Gangadhara (2005), caused by the retardation effect to  $\phi_j$ , i.e.  $\phi_j = \arctan(n_{\nu,y}/n_{\nu,x}) - \delta\phi_{\text{ret}}$ , where  $r_n = r/R_{LC}$  is the emission radius in units of the light cylinder radius and  $\theta_{\mu,j}$  is the half opening angle of the emission beam at the emission spot  $(\theta_j, \psi_j)$ .

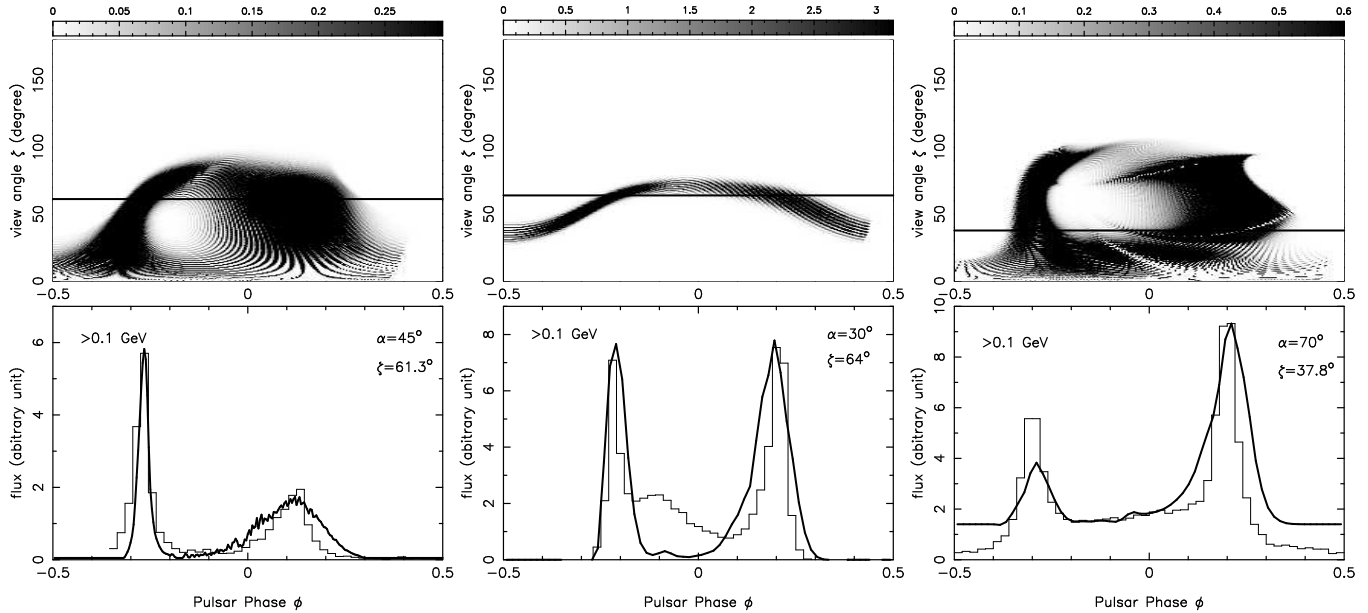
The ‘‘photon sky-map’’, and the corresponding light curve cut by a line of sight with a viewing angle  $\zeta$  are therefore finally derived. The application of the annular gap to young and millisecond pulsars for high energy pulse profiles are presented in Section 3.

### 3 SIMULATED LIGHT CURVES FOR YOUNG AND MILLISECOND PULSARS

Young  $\gamma$ -ray pulsars are very energetic, due to their large spin-down luminosity. The flux of gamma ray emission detected by EGRET are very high, e.g.,  $10^{-10} - 10^{-8} \text{ erg s}^{-1} \text{ s}^{-2}$  (Thompson et al. 1999). We use the annular gap model to simulate the light curves for the three brightest pulsars: the Crab, the Vela and the Geminga, respectively. The simulated light curves can reproduce the main observation features detected by Fermi (Abdo et al. 2010b). Most of the distinct light curves of millisecond pulsars detected by Fermi (Abdo et al. 2009a) can also

**Table 1.** The parameters for the simulated light curves for young and millisecond pulsars.

Pulsar	$\alpha$ ( $^\circ$ )	$\beta$ ( $^\circ$ )	$\lambda$	$\sigma$ ( $R_{LC}$ )	$\kappa$			
Crab	45	61.3	0.45	0.15	0.5 (> 0.1 GeV)	0.56 (> 1.0 GeV)	0.52 (0.3 – 1.0 GeV)	0.45 (0.1 – 0.3 GeV)
Vela	30	64	0.9	0.04	0.72 (> 0.1 GeV)	0.73 (> 1.0 GeV)	0.71 (0.3 – 1.0 GeV)	0.68 (0.1 – 0.3 GeV)
Geminga	70	37.8	0.7	0.22	0.68 (> 0.1 GeV)	0.73 (> 1.0 GeV)	0.7 (0.3 – 1.0 GeV)	0.46 (0.1 – 0.3 GeV)
J0030+0451	35	52.6	0.5	0.1	0.52 (> 0.1 GeV)			
J0218+4232	30	50	0.4	0.12	0.5 (> 0.1 GeV)			
J0437-4715	35	55	0.3	0.05	0.1 (> 0.1 GeV)			


**Figure 2.** The  $\gamma$ -ray photon sky-map (observer angle  $\zeta$  vs. rotation phase  $\phi$ ) and simulated light curves for the Crab pulsar (left panels), the Vela pulsar (middle panels) and the Geminga pulsar (right panels) in the framework of single-pole annular gap model, in comparison with the observations (thin solid lines, taken from Figure A-8, A-16 and A-12 of Abdo et al. 2010b). The simulated light curves are smoothed to 64 bins. The phase of magnetic pole in the photon sky-maps is set to be -0.15 to show the light curves in the middle. The observed light curves (thin solid lines) are compared with the simulated ones (thick solid lines). Parameters are given in Table 1.

be explained in the annular gap model, especially for pulse profiles of a single peak or small separation ( $\sim 0.2$  in phase). We have simulated three light curves of millisecond pulsars: PSR J0030+0451, PSR J0218+4232 and PSR J0437-4715, respectively. The relevant results will be briefly described below. The related parameters from simulations are given in Table 1.

### 3.1 The Crab pulsar

The Crab pulsar is famous for the phase-aligned pulse profiles of multi-wave band emission and beautiful X-ray torus. The observed  $\gamma$ -ray ( $>100$  MeV) features of the Crab pulsar (Abdo et al. 2010a and Abdo et al. 2010b) are two peaks with a separation of  $\sim 0.4$  rotation phase and a hard bridge. The observed light curves at different bands are quite similar. We simulated multi-band light curves for the Crab pulsar, but presented only one band in Figure 2 (left panels). It shows most of the observed features, especially for the phase-aligned pulse profiles with nearly similar peak ratio (P2/P1). An important result is that the  $\gamma$ -ray emission with higher photon energy comes from higher altitudes in the magnetosphere. This is probably caused by strong  $\gamma$ -B absorption effect for emission from lower altitudes (Lee et al. 2010). In addition, the parameters of  $\alpha$  and  $\zeta$  in our model are based on the adopted value (Wang 2003, Harding et al. 2008) and the results of X-ray torus simulation (Ng & Romani 2008). Other best  $\kappa$  and  $\sigma$  values indicate that the  $\gamma$ -ray photons are emitted from a wide range of emission altitudes from the neutron star surface to about half of the light cylinder radius.

### 3.2 The Vela pulsar

Similar to the Crab pulsar, the Vela pulsar is the brightest object in the  $\gamma$ -ray sky. Figure 2 (middle panels) shows the simulated light curve of  $> 0.1$  GeV band for the Vela pulsar. The main features, two sharp peaks with a separation of  $\sim 0.42$  and the peak ratio observed by Fermi and EGRET (Thompson 2001, Abdo et al. 2010b), are approximately reproduced. Similarly, we choose the parameters  $\zeta$  according to the

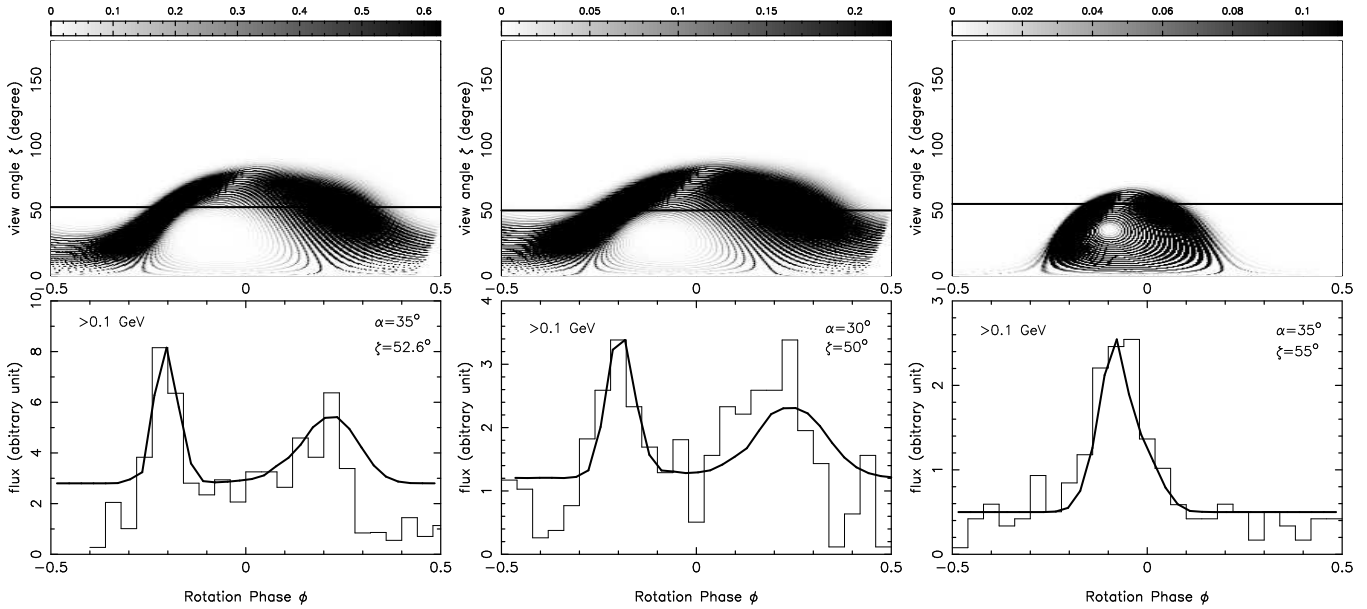


**Figure 3.** The same as Figure 2 but for the millisecond pulsar PSR J0030+0451 (left panels), PSR J0218+4232 (middle panels) and PSR J0437-4715 (right panels) in comparison with the observations (thin solid lines, taken from Figure A-2, A-4 and A-7 of Abdo et al. 2010b, respectively). The simulated light curves (thick solid lines) are smoothed to 32 bins.

result of X-ray torus simulation (Ng & Romani 2008). The inclination angle  $\alpha = 30^\circ$  which is thought to be an intermediate inclined rotator for the Vela gives the “best” simulated results. The best parameters  $\kappa$  and  $\sigma$  indicate that the  $\gamma$ -ray photons mainly come from high altitudes. Here we only used the open field lines in the annular gap region for the simulations. To get better results, especially for the third peak in the bridge, both the annular gap and core gap regions (Qiao et al. 2007) probably should be used to simulate the observed light curves for the Vela pulsar.

### 3.3 The Geminga pulsar

The Geminga pulsar is another bright  $\gamma$ -ray pulsar. Figure 2 (right panels) shows the simulated light curve for Geminga. The peak separation and peak ratio (Abdo et al. 2010b) are reproduced. The best  $\kappa$  and  $\sigma$  values indicate that the emission region could be mainly above the height of the null charge surface.

### 3.4 PSR J0030+0451

PSR J0030+0451 is a recently discovered solitary millisecond pulsar. The pulsed  $\gamma$ -ray emission was detected by Fermi (Abdo et al. 2009b). The simulated light curve ( $> 0.1$  GeV) for PSR J0030+0451 is shown in Figure 3 (left panels), which is similar to the observed features. The parameters  $\alpha$  is chosen for small magnetic inclination angles (Zhang et al. 1998, Tauris & Manchester 1998, Young et al. 2009). Furthermore, the  $\kappa$  and  $\sigma$  values indicate a small emission region at low altitudes.

### 3.5 PSR J0218+4232

The millisecond pulsar PSR J0218+4232 has a complex observed pulse profile (Figure A-4 of Abdo et al. 2010b). Figure 3 (middle panels) shows the simulated light curve ( $> 0.1$  GeV) for PSR J0218+4232. Our result roughly reproduces the observed peaks. The model parameters, similar to those of PSR J0030+0451, also favor a small emission region at low altitudes.

### 3.6 PSR J0437-4715

PSR J0437-4715 is the nearest millisecond pulsar with a good radio timing. It has a single narrow (about 0.2 phase) pulse peak at  $\gamma$ -ray band (Abdo et al. 2010b). Figure 3 (right panels) shows the simulated light curve for PSR J0437-4715. Our simulated result reproduces the features with a small inclination angle  $\alpha$  and a large viewing angle  $\zeta$ . Again, the model parameters are similar to those of PSR J0030-0451 and also favor a small emission region at low altitudes. Note that the  $\gamma$ -ray emission beams (photon sky-maps) of millisecond pulsars have a hollow cone in shape.

#### 4 DISCUSSIONS AND CONCLUSIONS

As an approximation, a static dipole field is used to model the pulsar magnetosphere. The pulsar magnetic field can be approximated by a static magnetic dipole configuration if the radial distance is not so far away from the pulsar surface (Muslimov & Harding 2005). The critical magnetic field lines used to define the annular gap are different in the magnetosphere models such as the retarded vacuum (Cheng et al. 2000) and force-free models (Spitkovsky 2006), since the positions of the null surface are different. However, in our model, the  $\gamma$ -ray emission regions are concentrated in the middle field lines of the annular gap, and the peak emission comes from the vicinity of the null charge surface. The high energy emission from the field lines near the upper boundary (critical field lines) and the ones near the lower boundary (last open field lines) give little contribution to the observed light curves. Our model is different from caustic models, e.g., the outer gap model, the slot gap model and the separatrix layer model (Bai & Spitkovsky 2009b), which all assumed a uniform emissivity along a field line. Our simulated light curves are mainly dependent on the non-uniform emissivities in a deformed radiation beam (see  $\lambda$  in equation 9) of the annular gap region.  $\lambda$  is described in detail in Lee et al. (2006), the large value leads to a more deformed radiation beam from the circle one. Owing to the intermediate height of  $\gamma$ -ray emission region, our annular gap model is weakly dependent on the magnetic field configuration either static or retarded dipole field.

The annular gap has a sufficient thickness of trans-field lines and high altitude acceleration regions. This leads to a fan-beam  $\gamma$ -ray emission and sufficient photon luminosity, which is suitable to interpret the observed light curves and the broad-band emission. The annular gap model holds the advantages of the slot gap and outer gap models, and works for pulsars with short spin periods. We use the annular gap model to simulate the light curves for young and millisecond pulsars with three assumptions: (i) the emissivities on a single field line between the critical field line and the last open field line follows a Gaussian distribution; (ii) the peak emission spot of a single field line is located at the vicinity of the null charge surface; (iii) the peak emissivities of a group of field lines with the same magnetic azimuthal (i.e., in the same plane) between the critical field line and the last open field line follows another Gaussian distribution. The assumption (ii) is consistent with our 1-D solution to the acceleration electric potential drop in the annular gap. The other two assumptions are mainly based on the magnetic pair absorption and the 3D global parallel electric field for the acceleration of relativistic charged particles in the magnetosphere, which will be investigated in future. In our calculations, it is shown that the emission region extends from the neutron star surface to about the half of the light cylinder radius, and our annular gap model is an intermediate emission height model. We also find the following conclusions from the modeling.

- (1) The simulated light curves can reproduce most of observed features for both young and millisecond pulsars. The  $\gamma$ -ray emission with higher photon energy comes from higher altitudes in the magnetosphere.
- (2) The  $\gamma$ -ray beams for both young and millisecond pulsars are hollow cones in shape.
- (3) The  $\gamma$ -ray emission light curves (pulse profiles) are determined by the inclination angle of magnetic dipole field and the observer's viewing geometry. The magnetic inclination angles and viewing angles of millisecond pulsars can not well constrained by any methods at present. This leads to difficulties for precise reproduction of light curves.
- (4) The radiation regions of young pulsars are larger. In terms of an individual field line, this large region covers from the pulsar surface to about the half of the light cylinder radius. The peak emission comes near the null charge surface.
- (5) The radiation regions of millisecond pulsars are small, from the pulsar surface to about the one third of the light cylinder radius. The peak emission comes from a region below the null charge surface.
- (6) Our model favors small inclination angles ( $\alpha \lesssim 35^\circ$ ) for the millisecond pulsars, and larger inclination angles ( $\alpha \sim 30^\circ - 70^\circ$ ) for the young pulsars. This is somewhat compatible with the alignment of the spin and magnetic axes over about 1 Myr from the analysis of the new pulsewidth data (Young et al. 2009).
- (7) Our results also show that the solid angle of gamma-ray beams are much less than  $4\pi$ , especially for MSPs. This will reduce the  $\gamma$ -ray emission conversion efficiency  $\eta = L_\gamma / \dot{E}_{\text{rot}}$ , and solve the puzzle for  $\eta > 1$  in Abdo et al. (2010b).

As shown in Qiao et al. (2004; 2007), the annular gap can have sufficient electric potential drop to produce pairs that can generate radio emission. Radio emission can be generated even at a higher region either for the annular gap or core gap. If radio emission comes from a lower region of either inner annular gap or the core gap (Qiao et al. 2004), the radio peak should appear between the two  $\gamma$ -ray peaks. On the other hand, it is possible that the radio radiation comes from a higher region or the opposite magnetic pole, producing a leading or trailing radio peak.

#### ACKNOWLEDGMENTS

The authors are very grateful to Mr. Xue-Ning Bai and the referee for valuable comments on the manuscript. We thank both the pulsar groups of NAOC and of Peking University for useful conversations. Especially, we appreciate Prof. Chou, Chih Kang for improving our presentation. The authors are supported by NSFC (10821061, 10573002, 10778611, 10773016 and 10833003) and the Key Grant Project of Chinese Ministry of Education (305001). K. J. Lee is also supported by ERC Grant "LEAP", Grant Agreement Number 227947.

## REFERENCES

- Abdo, A. A., et al. 2009a, *Science*, 325, 848  
 Abdo, A. A., et al. 2009b, *ApJ*, 699, 1171  
 Abdo, A. A., et al. 2009c, *Science*, 325, 840  
 Abdo, A. A., et al. 2010a, *ApJ*, 708, 1254  
 Abdo, A. A., et al. 2010b, *ApJS*, 187, 460  
 Arons, J. 1983, *ApJ*, 266, 215  
 Bai, X.-N., & Spitkovsky, A. 2009a, *ApJ*, in press (arXiv:0910.5741)  
 Bai, X.-N., & Spitkovsky, A. 2009b, *ApJ*, in press (arXiv: 0910.5740)  
 Cheng, K. S., Ho, C., & Ruderman, M. 1986a, *ApJ*, 300, 500  
 Cheng, K. S., Ho, C., & Ruderman, M. 1986b, *ApJ*, 300, 522  
 Cheng, K. S., Ruderman, M., & Zhang, L. 2000, *ApJ*, 537, 964  
 Chiang, J., & Romani, R. W. 1992, *ApJ*, 400, 629  
 Daugherty, J. K., & Harding, A. K. 1982, *ApJ*, 252, 337  
 Daugherty, J. K., & Harding, A. K. 1994, *ApJ*, 429, 325  
 Daugherty, J. K., & Harding, A. K. 1996, *ApJ*, 458, 278  
 Dyks, J., & Rudak, B. 2003, *ApJ*, 598, 1201  
 Dyks, J., & Harding, A. K. 2004, *ApJ*, 614, 869  
 Frackowiak, M., & Rudak, B. 2005, *Memorie della Societa Astronomica Italiana*, 76, 523  
 Gangadhara, R. T. 2004, *ApJ*, 609, 335  
 Gangadhara, R. T. 2005, *ApJ*, 628, 923  
 Goldreich, P., & Julian, W. H. 1969, *ApJ*, 157, 869  
 Gruzinov, A. 2007, *ApJL*, 667, L69  
 Harding, A. K., Stern, J. V., Dyks, J., & Frackowiak, M. 2008, *ApJ*, 680, 1378  
 Hirotani, K., Harding, A. K., & Shibata, S. 2003, *ApJ*, 591, 334  
 Hirotani, K. 2008, *ApJL*, 688, L25  
 Komissarov, S. S. 2006, *MNRAS*, 367, 19  
 Lee, K. J., Qiao, G. J., Wang, H. G., & Xu, R. X. 2006, *Advances in Space Research*, 37, 1988  
 Lee, K. J., Cui, X. H., Wang, H. G., Qiao, G. J., & Xu, R. X. 2009, *ApJ*, 703, 507  
 Lee, K. J., Du, Y. J., Wang, H. G., Qiao, G. J., Xu, R. X., & Han, J. L. 2010, *MNRAS*, in press  
 Lin, G. F., & Zhang, L. 2009, *ApJ*, 699, 1711  
 McKinney, J. C. 2006, *MNRAS*, 368, L30  
 Muslimov, A. G., & Harding, A. K. 2003, *ApJ*, 588, 430  
 Muslimov, A. G., & Harding, A. K. 2004, *ApJ*, 606, 1143  
 Muslimov, A. G., & Harding, A. K. 2005, *ApJ*, 630, 454  
 Ng, C.-Y., & Romani, R. W. 2008, *ApJ*, 673, 411  
 Pellizzoni, A., et al. 2009, *ApJL*, 695, L115  
 Qiao, G. J., Lee, K. J., Wang, H. G., Xu, R. X., & Han, J. L. 2004, *ApJL*, 606, L49  
 Qiao, G. J., Lee, K. J., Zhang, B., Wang, H. G., & Xu, R. X. 2007, *Chinese Journal of Astronomy and Astrophysics*, 7, 496  
 Romani, R. W. 1996, *ApJ*, 470, 469  
 Romani, R. W., & Yadigaroglu, I.-A. 1995, *ApJ*, 438, 314  
 Ruderman, M. A., & Sutherland, P. G. 1975, *ApJ*, 196, 51  
 Spitkovsky, A. 2006, *ApJ*, 648, L51  
 Tang, A. P. S., Takata, J., Jia, J. J., & Cheng, K. S. 2008, *ApJ*, 676, 562  
 Tauris, T. M., & Manchester, R. N. 1998, *MNRAS*, 298, 625  
 Timokhin, A. N. 2006, *MNRAS*, 368, 1055  
 Thompson, D. J., et al. 1999, *ApJ*, 516, 297  
 Thompson, D. J. 2001, *American Institute of Physics Conference Series*, 558, 103  
 Venter, C., Harding, A. K., & Guillemot, L. 2009, *ApJ*, 707, 800  
 Wang, H. G. 2003, PhD thesis, Peking University  
 Wang, H. G., Qiao, G. J., Xu, R. X., & Liu, Y. 2006, *MNRAS*, 366, 945  
 Watters, K. P., Romani, R. W., Weltevrede, P., & Johnston, S. 2009, *ApJ*, 695, 1289  
 Xu, R. X. 2002, *ApJL*, 570, L65  
 Xu, R. X. 2005, *MNRAS*, 356, 359  
 Young, M. D. T., Chan, L. S., Burman, R. R., & Blair, D. G. 2010, *MNRAS*, 402, 1317  
 Zhang, L., & Cheng, K. S. 1997, *ApJ*, 487, 370

Zhang, C. M., Cheng, K. S., & Wu, X. J. 1998, A&A, 332, 569

Zhang, L., Cheng, K. S., Jiang, Z. J., & Leung, P. 2004, ApJ, 604, 317

Zhang, H., Qiao, G. J., Han, J. L., Lee, K. J., & Wang, H. G. 2007, A&A, 465, 525